Desalination and Water Treatment
www.deswater.com
doi: 10.1080/19443994.2014.993718

57 (2016) 4049–4058
February

Taylor & Francis
Taylor & Francis Group

Selective separation of Pb^{2+} from aqueous solutions by a novel imprinted adsorbent

S. Ghoohestani, H. Faghihian*

Department of Chemistry, Islamic Azad University, Shahreza Branch, Shahreza, Iran, email: Sh_ghoohestani@yahoo.com (S. Ghoohestani), Fax: +983213213015; email: Faghihian@iaush.ac.ir (H. Faghihian)

Received 5 May 2014; Accepted 7 November 2014

ABSTRACT

In this research, a selective ion-imprinted adsorbent was synthesized by polymerization of chitosan on the MCM-41 surface. The adsorbent was characterized by FTIR, X-ray diffractometer, and TG/DTG techniques. The surface area, pore size, and pore volume of the adsorbent were calculated by nitrogen adsorption–desorption isotherms. The adsorbent was used for selective separation of Pb^{2+} from aqueous solutions. The effect of different experimental conditions on the adsorption capacity was examined and the optimized conditions were determined: pH 5.5; contact time, 60 min; temperature, 298 K; Pb^{2+} concentration, 250-mg L^{-1}; and adsorbent dose, 0.1-g. The maximum adsorption capacity was 57.7 and 27-mg g^{-1}, respectively, for ion-imprinted and non–ion imprinted adsorbents. The removal efficiency for ion-imprinted sample was 92%. Breakthrough adsorption capacity was measured as 50.75 and close to the static adsorption capacity. The relative selectivity factor for Pb^{2+}/Cd^{2+} and Pb^{2+}/Ni^{2+} pairs were, respectively, 52.43 and 80.56. The relative standard deviation of the method was 1.12% for 10 replicate samples. The data collected from the adsorption isotherms was fitted to the Langmuir equation.

Keywords: Adsorbent; Selective removal; Pb^{2+}; Adsorption; Chitosan; MCM-41

1. Introduction

The monitoring and remediation of heavy metal pollution is increasingly becoming a crucial global issue since heavy metals can cause many biological abnormalities and tend to accumulate in food chains [1–4]. Among heavy metals, lead (Pb), with important environmental and toxicological significance, has become a research hotspot and received wide concerns [5]. Various kinds of methods are available for the determination and/or removal of Pb^{2+} in water samples [6]. For example, Pan et al. have fabricated a nanomaterial–ionophore-based electrode for anodic stripping voltammetric detection of Pb^{2+} [7]. So the development of selective separation and detection methods for trace amounts of lead ions has attracted widespread attention [8]. However, the presence of complex matrices in environmental samples is generally a huge obstruction to performing direct analysis of Pb^{2+}. Although a number of methods such as membrane and chemical precipitation, and ion exchange are industrially suitable for nonpreferential separation of heavy metal ions, the poor selective separation is still a large defect [9]. Therefore, it is urgently required to develop highly selective separation/removal materials and methods for Pb^{2+}. Meanwhile,

*Corresponding author.

molecular imprinting is a commonly used technology to build a molecular recognition mechanism in triaxial cross-linked polymers named: molecularly imprinted polymers (MIPs) [10]. More recently, MIPs have been identified as ideal materials and are widely used in contaminant removal and trace analysis, since they are suitable for applications where analyte selectivity is essential [10–12]. Ion-imprinted polymers (IIPs), an important branch of MIPs, are similar to MIPs. By ion-imprinting method, tailor-made materials can be prepared through polymerizing suitable monomers in the presence of a desired imprinted ion and they recognize inorganic ions after imprinting, especially metal ions. A number of IIPs for metal ions have been prepared and applied to the determination and removal, such as Pb^{2+} IIPs [13–16]. Among present ion-imprinted techniques, imprinting of a matrix with binding sites situated at the surface has many advantages such as more accessible sites, easier mass transfer, and faster binding kinetics [17,18]. Silica-based mesoporous materials have been universally reported as good solid support due to their structural, chemical and mechanical stability, and well modified surface properties with abundant Si–OH active bonds [19–21]. Among the mesoporous silica, MCM-41 is characterized with ultra large pore diameters, large surface area, high pore volume, thicker pore walls, and excellent homogeneity that enables itself as a potential candidate for inclusion of guest species on the surface [22,23]. Chitosan (CTS) is an N-deacetylated product of chitin and the second most abundant natural biopolymer after cellulose. This natural polymer and its derivatives have received great attention for metal adsorption due to the high ratio of hydroxyl and amine groups [24]. However, the poor mechanical and chemical stability of pure CTS limits its applications. Coating CTS on silica-based mesoporous materials with chemical cross-linking process has been considered a successful method [25]. In this study, a novel lead ion-imprinted adsorbent was prepared by the polymerization of CTS as a functional monomer on the MCM-41 support matrix. The adsorption behavior of the synthesized adsorbent for removal of Pb^{2+} from aqueous solutions was studied and the results were discussed.

2. Experimental

2.1. Reagents and instruments

MCM-41 (Mobil Composition of Matter No. 41), CTS, degree of deacetylation more than 90% (Aldrich), KH-560 (3-(2,3-epoxypropoxy) propyltrimethoxysilane) (Merck), cetyltrimethylammonium bromide (CTAB) 98%, aqueous ammonia (25% NH_3), and tetraethoxysilane (TEOS) 98% (Merck) were employed for synthesis of the adsorbent. Standard stock solutions of Pb^{2+} were prepared by $Pb(NO_3)_2$ using deionized water. All the chemicals used were of analytical grade.

The infrared spectra (FTIR 4,000–400 cm^{-1}, KBr pellet) were recorded by a Perkin Elemer-65. D-8 ADVANCE X-ray diffractometer (XRD) (Bruker, Germany) was used to prepare the XRD pattern of the sample with CuKα radiation ($\lambda = 0.1541$ nm). BET surface area was measured using a BEL-max adsorption surface analyzer (Japan). Cation concentration was measured with an Analyst 300 flame atomic adsorption spectrometer (FAAS) (Perkin Elemer), and thermal curves were recorded by TG-DSC Setaram instrument (Germany).

2.2. Synthesis of lead-imprinted adsorbent

MCM-41 was prepared according to the procedure described by Heidari et al. [22]. The synthesized material was activated by refluxing with 3 M hydrochloric acid for 24 h. The treated sample was separated and thoroughly washed with deionized water. The polymer suspension was prepared by adding 5.0 g CTS and 2.0 g $Pb(NO_3)_2$ $6H_2O$ into 160.0 mL of 0.1 M acetic acid solution. After stirring for 1 h, 40 mL of KH-560 was added into the mixture and stirred for 5 h at 25°C. The product was thoroughly dispersed by ultrasonic radiations, and 16.5 g of activated MCM-41 was added into the mixture. Stirring was continued for 3 h until the polymer was formed on the substrate surface. The wet product was dried at room temperature and treated with 3 M HNO_3 to remove the coordinated Pb^{2+}. After neutralization with 0.2 M NaOH solution, the adsorbent was dried at 70°C under vacuum, grinded, and sieved. The resulting ion-imprinted polymer was designated as IIP. Non ion-imprinted polymer (NIP) was prepared in the same way without the addition of $Pb(NO_3)_2{\cdot}6H_2O$.

2.3. Adsorption experiments

Batch experiments were conducted to study the adsorption behavior of the adsorbent by adding 0.1 g of IIP into 25 mL lead solution (250 mg L^{-1}). The pH of the solution was adjusted to 5.5 (by adding 0.1 M NaOH solution), and the mixture was shaken for 1 h. The solid was separated by centrifugation and the concentration of the Pb^{2+} in the solution was determined by FAAS. The adsorption efficiency (E%) and absorption capacity (Q, mg g^{-1}) were, respectively, calculated by Eqs. (1) and (2):

$$E\% = (C_0 - C)/C_0 \times 100 \quad (1)$$

$$Q = ((C_0 - C)V)/W \quad (2)$$

where C_0 and C are, respectively, the initial and equilibrated concentrations of Pb^{2+} (mg L^{-1}), V is the volume of the solution (L) and W is the mass of adsorbent (g).

Column adsorption experiments were conducted by a column (inner diameter of 9 and 500 mm length) packed with 40 mg of the imprinted polymer. A small amount of glass wool was placed at both the ends of the column to prevent loss of the particles during sample loading. Before use, the column content was cleaned and neutralized by passing deionized water through the column. Then, lead solution was passed through the column at a flow rate of 0.2 mL min^{-1}. The metal ion adsorbed by the adsorbent was eluted with 25 mL of 2 M HNO_3 solution. The Pb^{2+} concentration in the eluted solution was measured by FAAS. The breakthrough curve was constructed and the dynamic capacity was calculated.

2.4 Selectivity of the adsorbent

In order to measure the selectivity of the adsorbents, competitive adsorption of Pb^{2+}/M (M: Other metal ions) was studied for IIP and NIP. The distribution coefficients K_d (mL g^{-1}), selectivity coefficient (k), and the relative selectivity coefficient k' were calculated by the following equations:

$$K_d = (C_i - C_f)/C_f W \quad (3)$$

$$k = K_{dPb}/K_{dM} \quad (4)$$

$$k' = k_{IIP}/k_{NIP} \quad (5)$$

where C_i and C_f represent, respectively, the initial and equilibrated concentrations of the given metal ions in the solution. K_d (Pb) and K_d (M) represent, respectively, the distribution coefficients of Pb^{2+} and M ions. $k_{(IIP)}$ and $k_{(NIP)}$ represent the selectivity coefficient of Pb^{2+}-IIP and NIP.

2.5. Regeneration of the adsorbent

To regenerate the used sample, it was eluted with 3 M HNO_3, washed with deionized water, and dried under vacuum. The regenerated adsorbent was reused for Pb^{2+} adsorption. The adsorption–desorption process was repeated for five successive cycles and the adsorption rate for each cycle was calculated.

3. Results and discussion

3.1. Characterization of the samples

The FTIR spectra of the samples are shown in Fig. 1. The wide and strong adsorption band at 3507.7 cm^{-1} is ascribed to the stretching vibrations of N–H and O–H of CTS (Fig. 1(a)). This characteristic absorption bands shifted to 3407.8 cm^{-1} after –N and –O were coordinated with Pb^{2+}. In the FTIR of Pb–CTS (Fig. 1(b)), the bending vibration of $-NH_2$ at 1,659 cm^{-1} and stretching vibrations of –OH at 1,082 cm^{-1} of CTS were, respectively, shifted to 1,645 and 1,061 cm^{-1}, confirming the formation of Pb–N and Pb–O bonds on the surface of the adsorbent [26]. The absorption bands observed at 803 and 1089.5 cm^{-1} were, respectively, attributed to the stretching vibration, antisymmetric stretching vibration of Si–O tetrahedron of the MCM-41 structure (Fig. 1(c)). The absorption band at 1,617 cm^{-1} was assigned to in-plane bending vibration of Si–OH. The broad absorption peak at 3,441 cm^{-1} was considered as the vibration absorption of surface Si-OH. As a result of co-condensation between silanols from self-hydrolysis of siloxane and –OH from MCM-41, the Si–O–Si band appeared at 1,085, confirming that the polymer was grafted on the substrate surface (Fig. 1(d)). In the FTIR spectrum of the leached sample, the O–H and N–H bands were recovered and became sharper. This envisaged that the template ions were removed after eluting with acid and the bonds between Pb^{2+}, O–H, and N–H groups were eliminated (Fig. 1(e)).

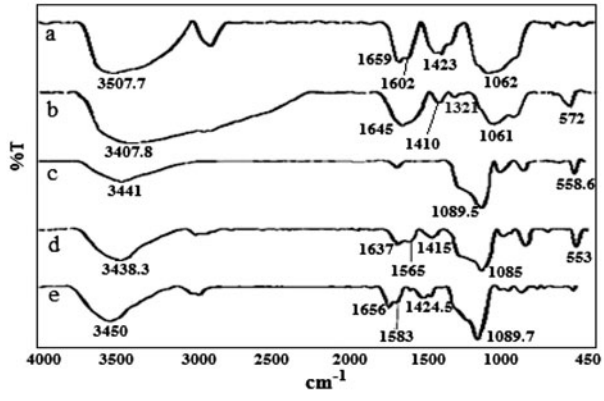

Fig. 1. Infrared spectra of CTS (a), CTS+Pb^{2+} (b), MCM-41 (c), Pb^{2+}-imprinted polymer with Pb^{2+} (d), and Pb^{2+}-imprinted polymer (e).

In the XRD pattern of MCM-41, four diffraction lines were observed at 2.44, 4.20, 4.83, and 6.35, which are the characteristic lines of the material (Fig. 2(a)) [27]. In the XRD pattern of the Pb^{2+}-IIP, the diffraction line observed at 2.57° indicated that the structure of MCM-41 remained unchanged (Fig. 2(b)). The decrease in the intensity of the lines at 4.20, 4.83, and 6.35 lines provided evidence that grafting mainly occurred inside the channels and the attachment of organic functional groups in the mesopore channels reduced the scattering power of the mesoporous silicate walls.

The data calculated from nitrogen adsorption–desorption isotherms of the samples are summarized in Table 1. After polymerization, due to grafting (Fig. 3), of the polymer on the mesoporous channel, the surface area and the total pore volume of MCM-41 were significantly decreased. The average pore size of MCM-41 and ion-imprinted sample was very close indicating that polymerization has only little effect on the particle growth.

Thermal curves (DTG) were obtained at linear heating rates of 20 °C min^{-1} from ambient temperature to 700 °C under nitrogen atmosphere (Fig. 4). In the thermal curve of MCM-41, a single weight loss peak was observed around 100 °C which was attributed to the dehydration of water molecules adsorbed on the surface of the sample (Fig. 4), while in the thermal curve of Pb^{2+}-imprinted sample two distinct weight loss peaks were observed, respectively, at 91.9 and 196.4 °C. The second peak was attributed to the decomposition of the polymer. The weight percent of the polymer grafted on the MCM-41surface was estimated by this peak as 25%W.

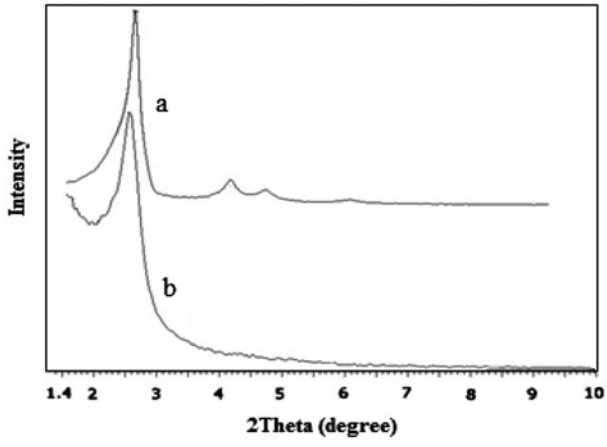

Fig. 2. XRD pattern: (a) MCM-41 and (b) Ion-imprinted adsorbent.

3.2. Adsorption experiments

The influence of pH on the adsorption of lead was studied at pH ranges of 1.0–5.5 (Fig. 5). The insignificant adsorption capacity obtained at lower pHs was attributed to the protonation of adsorption sites and also competition of hydrogen ions with lead for adsorption sites [28,29], Eq. (6).

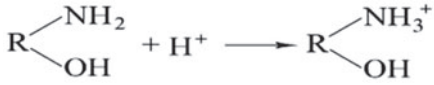

(6)

The adsorption capacity was increased by increasing the pH of the solution and the optimized capacity was obtained at pH 5.5. At pH higher than 5.5 Pb^{2+} was precipitated as $Pb(OH)_2$. The adsorption mechanism is assumed to be chemical in nature. Two adjacent amino groups and two hydroxyl groups give two pairs of electrons to the metal ions and form four coordination number compounds [30], Eq. (7).

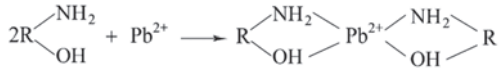

(7)

For regeneration of the adsorbent, HNO_3 solution (3 M) was used. It is assumed that, H^+ replaced lead ions through ion-exchange mechanism, Eq. (8).

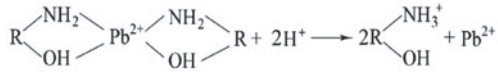

(8)

Other metal ions did not fix to the tailored adsorption sites. Therefore, IIP was a selective adsorbent for Pb^{2+}. According to selectivity experiment, the selectivity mainly was controlled by the shape of cavities (the size of the metal ions) and coordination geometry [31].

Low temperature was in favor for Pb^{2+} adsorption onto IIP, the adsorption capacity of the ion-imprinted sample decreased by increasing the temperature from 25 to 55 °C (Fig. 6(a)). With the rise in temperature and by weakening the adsorptive forces between the active sites and the lead ions, the tendency of the Pb^{2+} ions to escape from the solid phase to the bulk of solution increased. The reverse effect was observed for the NIP sample (Fig. 6(b)).

To study the effect of adsorbent dose on the adsorption efficiency, 50 mL of Pb solution (100 mg L^{-1}) was contacted with different amounts of the adsorbent under optimized conditions. The solid was separated after 1 h and the concentration of Pb was measured in the filtrate. The maximal adsorption capacity was observed with 0.1 g of the adsorbent (Fig. 7(a)).

Table 1
Pore characterization of MCM-41 and Pb^{2+}-IIP

Samples	Surface area ($m^2 g^{-1}$)	Pore volume ($cm^3 g^{-1}$)	Average pore diameter (nm)
MCM-41	1073	0.93	3.46
Pb^{2+}-IIP	189	0.17	3.65

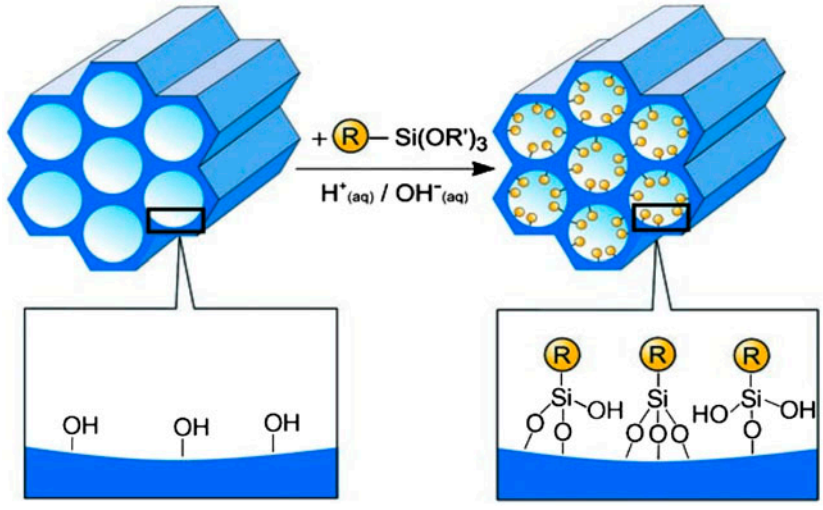

Fig. 3. Grafting of the polymer on the MCM-41 channel with terminal organosilanes of the type $(R'O)_3$ SiR. *R*=organic functional group (CTS).

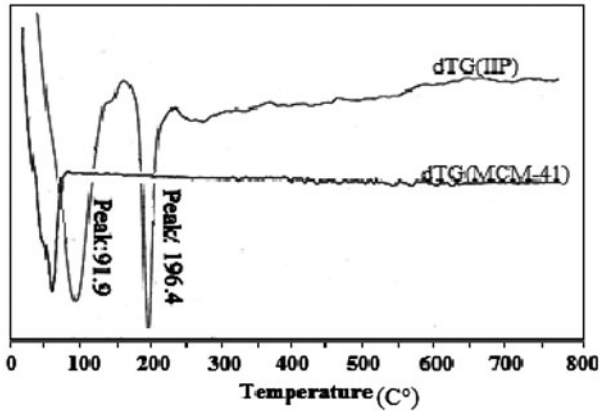

Fig. 4. DTG pattern of MCM-41 and Pb^{2+}-imprinted adsorbent.

3.3. Adsorption kinetics

The adsorption rate increased rapidly during the initial 50 min, and then reached equilibration after 1 h (Fig. 7(b)). The fast kinetics of adsorption envisaged that the IIP was suitable for preconcentration of Pb^{2+} by continuous column separation from large volumes of the solution. To examine the kinetics of the adsorption process, Lagergren's pseudo-first-order kinetic model [Eq. (9)] and second-order kinetic model [Eq. (10)] were applied:

$$\log(Q_{max}) = \log Q_{max} - (k_1/2.303)t \quad (9)$$

$$t/Q_t = 1/k_2 Q_{max}^2 + (1/Q_t) \quad (10)$$

where q_t and q_{max} (mg g^{-1}) are the adsorption capacity at t and equilibrium time (min), k_1 (min^{-1}) and k_2 (g (mg min)$^{-1}$) are pseudo-first- and second-order rate constants, respectively (Fig. 8(a) and (b)). Pseudo-first-order model rendered the rate of occupied adsorption sites to be proportional to the number of unoccupied sites; and pseudo-second-order-kinetic model assumed that the chemical reaction mechanisms [32, and that the adsorption rate is controlled by chemical adsorption through sharing or exchange of electrons between the adsorbent and adsorbate [33]. As shown in Table 2, the correlation coefficient for the pseudo-second-order model was higher than the first order. Therefore, the adsorption of Pb^{2+} on IIP agreed well to the

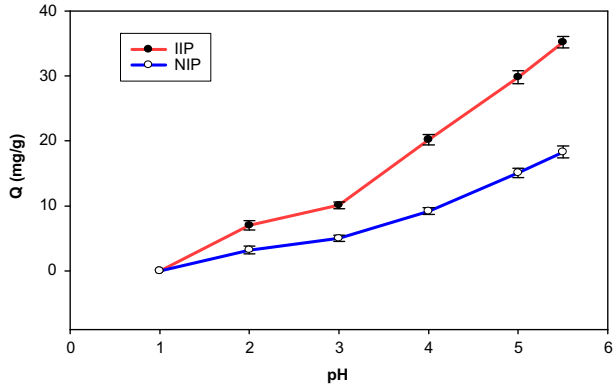

Fig. 5. Effect of pH on Pb^{2+} adsorption conditions: Sorbent = 0.1 g; Pb^{2+} conc. = 100 mg L^{-1}; shaking time = 10 min; adsorption time = 1.0 h; temperature = 25 ℃.

second-order kinetic model, indicating that the adsorption process was a chemical process.

3.4. Adsorption isotherm

Adsorption capacity increased with initial concentration of Pb^{2+} and after a certain concentration, owing to the lower active sites being available, the equilibration was attained (Fig. 9). The isotherms data were examined with the Langmuir adsorption isotherm [Eq. (11)]

$$C_e/q_e = 1/q_m K_L + C_e\,(1/q_m) \quad (11)$$

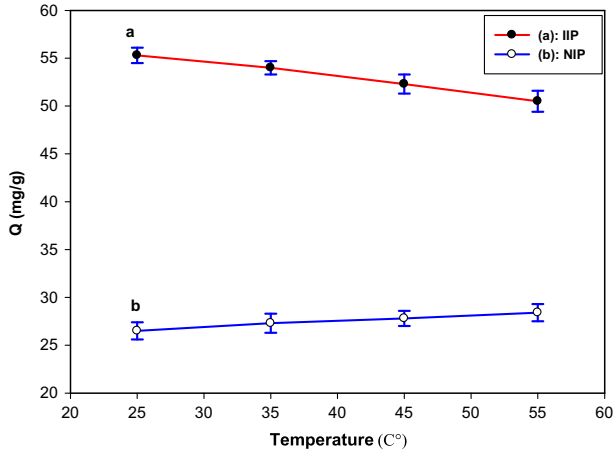

Fig. 6. Effect of temperature on Pb^{2+} adsorption conditions: sorbent = 0.1 g; pH 5.5, Pb^{2+} conc. = 250 mg L^{-1}; shaking time = 10 min; adsorption time = 1.0 h.

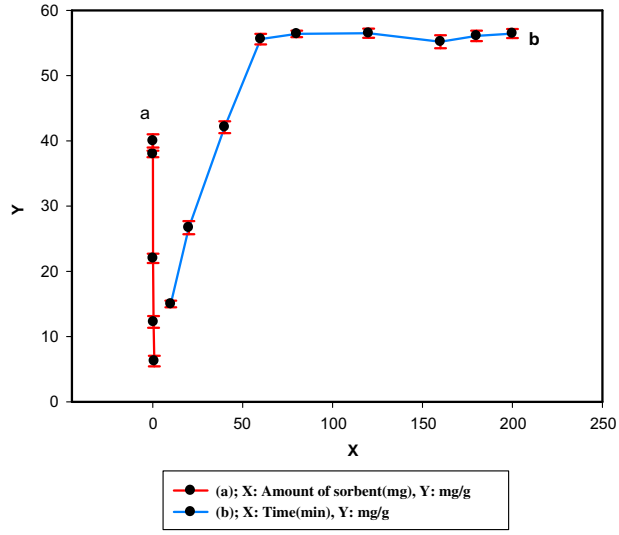

Fig. 7. (a) Effect of amount of IIP on Pb^{2+} adsorption. Conditions: pH 5.5; Pb^{2+} conc. = 100 mg L^{-1}; shaking time = 10 min; adsorption time = 1.0 h; temperature = 25 ℃ and (b) Kinetic of adsorption. Conditions: IIP = 0.1 g; Pb^{2+} conc. = 250 mg L^{-1}; shaking time = 10 min; temperature = 25 ℃.

where C_e (mg L^{-1}) and q_e (mg g^{-1}) are the adsorption capacities at the different initial concentrations of Pb^{2+}, and K_L (L mg^{-1}) is the adsorption–desorption equilibrium constant related to the binding energy. According to the Langmuir model (Fig. 10) adsorption occurred uniformly on the active sites of the adsorbent. Once a, adsorbate occupied the site, no further adsorption could take place at this site [34]. The experimental data well fitted with the Langmuir adsorption isotherm model, as shown in Table 3. Therefore, the

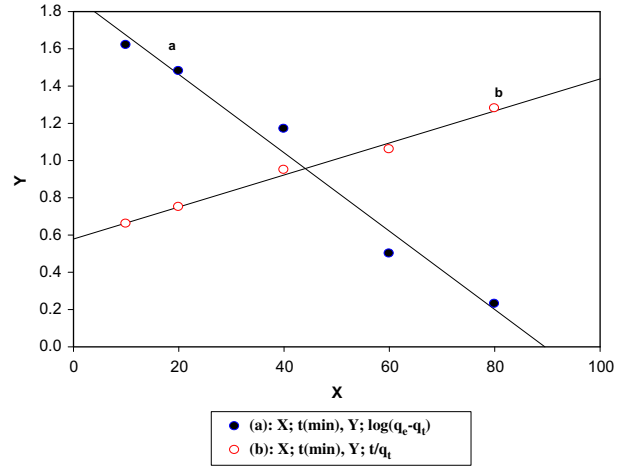

Fig. 8. (a) Lagergren pseudo-first-order kinetic model and (b) Pseudo-second-order kinetic model.

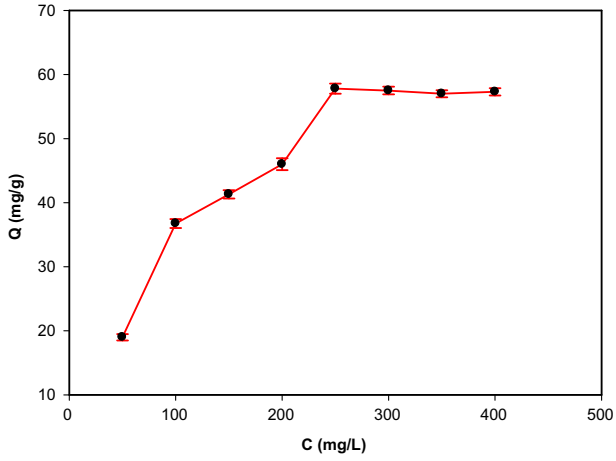

Fig. 9. Adsorption isotherms for Pb^{2+} adsorption onto IIP sample. Conditions: IIP = 0.1 g; pH 5.5, shaking time = 10 min; temperature = 25°C.

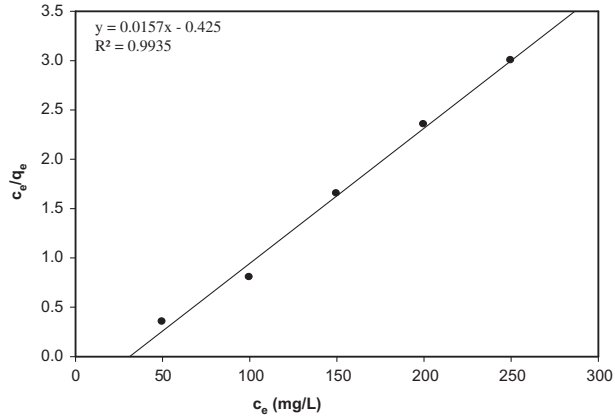

Fig. 10. Adsorption of Pb^{2+} onto Pb^{2+}-IP using Langmuir model.

Table 2
Lagergren pseudo first- and second-order kinetic data of MCM-41-IIP(IIP)

Model	Parameters			R^2
Pseudo-first-order	k_1 (min^{-1}) = 0.0121	Q_{exp} (mg g^{-1}) = 56.7	Q_{Cal} (mg g^{-1}) = 76	0.9564
Pseudo-second-order	k_2 (g mg^{-1} min^{-1}) = 0.8756	Q_{exp} (mg g^{-1}) = 56.7	Q_{Cal} (mg g^{-1}) = 62.5	0.9952

Table 3
Langmuir and Freundlich adsorption isotherm data for Pb^{2+} adsorption onto Pb^{2+}-imprinted polymer

Freundlich				Langmuir		
R^2	K_F	n	R_L	R^2	K_L (L mg^{-1})	q_m (mg g^{-1})
0.8916	8.52	2.55	0.004	0.9935	0.114	62.5

adsorption process could be considered as a mono–layer adsorption. For predicting the favorability of an adsorption system, the Langmuir equation can also be expressed in terms of a dimensionless separation factor R_L (Eq. (12)) [35,36].

$$R_L = 1/(1 + K_L C_o) \quad (12)$$

where R_L indicates the favorability and the capacity of the adsorbent/adsorbate system. When $0 < R_L < 1$, it represents good adsorption. As shown in Table 3, the present adsorption systems were favorable and the adsorption of Pb^{2+} was more favorable at higher initial Pb^{2+} concentrations than at lower concentrations. From the results, it was a indicated that the imprinted polymer supported by MCM-41 was much more efficient adsorbent than NIP. Moreover, the saturation adsorption capacity in the present work is higher than the values reported for Pb^{2+} adsorption on Pb^{2+}-IIP prepared by bulk polymerization [37], Pb^{2+}-imprinted amino-functionalized silica gel (19.66 mg g^{-1}) [38], and Pb^{2+}-IIP on nano-TiO_2 matrix [39]. The high adsorption capacity in this research can be explained as

Table 4
Effect of imprinting on selectivity

k'	K_{NIP}	K_{IIP}	Interfering ions
80.56	1.77	142.6	Ni^{2+}
52.43	7.30	382.8	Cd^{2+}

Table 5
Optimized conditions for adsorbent recovery

Conc. (mol L^{-1})	Recovery (mg g^{-1})	Volume (mL)	Recovery (mg g^{-1})	Shaking time (min)	Recovery (mg g^{-1})
0.5	74.7	5	74.3	10	65.8
1	80.7	10	97.6	20	74.5
2	85.5	15	96.1	40	83.5
3	96.3	20	98.5	80	98.7

follows: When the Pb ions of the polymer grafted onto the surface of the inner channel of MCM-41 with high surface area, is leached out, enough cavities are left on the surface and act as adsorption sites of the adsorbent.

3.5. Breakthrough capacity

The data for plotting of breakthrough curve were obtained by pumping Pb^{2+} solution (20 mg L^{-1}, pH 5.5) through the column (explained in section. 2.3) at the flow rate of 0.2 mL min^{-1}. The column effluent was continuously collected at each 25 mL portion and the concentration of Pb^{2+} was measured by FAAS. The extraction ratio (C_e/C_i, where C_e and C_i are the analyte concentration in the outgoing and ingoing solutions, respectively) was plotted against the volume of effluent (Fig. 11). The breakthrough capacity was calculated with the assumption that the breakthrough occurred at $C_e/C_i = 0.01$. It was found to be 50.75 mg g^{-1} and close to the optimized capacity of the adsorbent obtained by batch experiments (57.7 mg g^{-1}). The result of this experiment showed that the synthesized adsorbent can be used for preconcentration of lead by use of column operation.

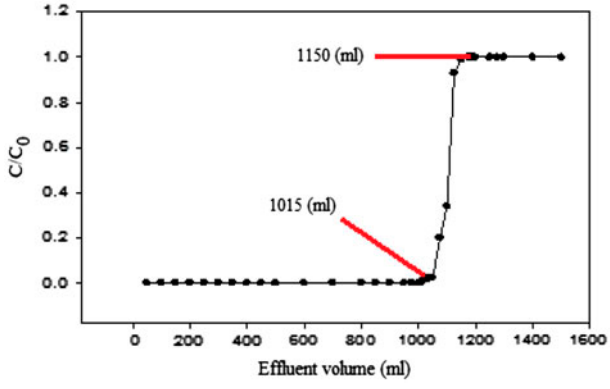

Fig. 11. Breakthrough volume curve. Conditions: Pb^{2+} conc. = 20 mg L^{-1}; IIP = 0.4 g; pH 5.5; Flow = 0.2 mL min^{-1}.

3.6. Adsorption selectivity

Competitive adsorption rates of the same charge or similar ionic radii ions such as Pb^{2+}/Ni^{2+} and Pb^{2+}/Cd^{2+} from their mixtures were investigated by using Pb^{2+}-IIP and NIP. As shown in Table 4, the K_d (IIP) value of ion–imprinted adsorbent for Pb^{2+} was larger, while K (IIP) decreased significantly for Cd^{2+} and Ni^{2+}, while NIP has low k value due to the random distribution of ligand functionalities in the polymeric network, whereas in the case of Pb^{2+}-IP, the cavities created after the removal of the template were complementary to the imprint ion in size, shape, and coordination geometries. It was demonstrated that Pb^{2+}-IP synthesized for Pb^{2+} had higher selectivity (k': Relative selectivity coefficient) for this ion.

3.7. Regeneration of the adsorbent

Since the adsorbent showed very low capacity for Pb^{2+} at acidic pH (Fig. 5), it was concluded that the adsorbed Pb^{2+} can be eluted by acidic solutions (HNO_3). The effect of HNO_3 concentration, HNO_3 volume, and shaken time on Pb^{2+} recovery was evaluated. The recovery rate increased gradually with the rise in HNO_3 concentration and HNO_3 volume. The full recovery was achieved with 10 mL of 3 M HNO_3 and shaking time of 80 min (Table 5). The regeneration of the adsorbent was studied for five consecutive adsorption–desorption cycles. The results indicated that the adsorbent retained 94.63% of its original capacity after the last regeneration cycle (Table 6).

Table 6
Adsorption–desorption cycles

% Regeneration	Adsorbtion capacity (mg g^{-1})	Regeneration cycles
100.0	0.96 ± 56.64	1
97.8	0.56 ± 55.4	2
97.1	0.92 ± 55.02	3
95.02	1.03 ± 53.82	4
94.63	1.11 ± 53.60	5

4. Conclusions

In this study, a novel selective adsorbent was prepared by surface imprinting Pb^{2+}-CTS on the MCM-41 surface. The ion-imprinted polymer was used for the removal of Pb^{2+} from aqueous solutions. Compared to other adsorbents, the synthesized composite showed high adsorption capacity and selectivity towards the studied cation. The regeneration of the adsorbent showed that 94.63% of the original capacity remained after five successive regeneration cycles. The adsorption process was kinetically fast and application of the adsorbent in column operation is quite feasible.

References

[1] H.A. Naser, Assessment and management of heavy metal pollution in the marine environment of the Arabian Gulf: A review, Mar. Pollut. Bull 72 (2013) 6–13.

[2] F.L. Fu, Q.J. Wang, Removal of heavy metal ions from wastewaters: A review, J. Environ. Manage. 92 (2011) 407–418.

[3] A. Nzihou, B.J. Stanmore, The fate of heavy metals during combustion and gasification of contaminated biomass: A brief review, J. Hazard. Mater. 256–257 (2013) 56–66.

[4] I.R. Pala, S.L. Brock, ZnS nanoparticle gels for remediation of Pb^{2+} and Hg^{2+} polluted water, ACS Appl. Mater. Interfaces 4 (2012) 2160–2167.

[5] M.R. Sohrabi, Z. Matbouie, A.A. Asgharinezhad, A. Dehghani, Determination of Aflatoxins in rice samples by ultrasound-assisted matrix solid-phase dispersion, Microchim. Acta 180 (2013) 589–597.

[6] R. Rehman, J. Anwar, T. Mahmud, Sorptive removal of lead (II) from water using chemically modified mulch of Madhuca longifolia and Polyalthia longifolia as novel biosorbents, Desalin. Water Treat. 51 (2013) 2624–2634.

[7] D.W. Pan, Y. Wang, Z.P. Chen, T.T. Lou, W. Qin, Nanomaterial/ionophore-based electrode for anodic stripping voltammetric determination of lead: An electrochemical sensing platform toward heavy metals, Anal. Chem. 81 (2009) 5088–5094.

[8] A.R. Timerbaev, Element speciation analysis using capillary electrophoresis: Twenty years of development and applications, Chem. Rev. 113 (2013) 778–812.

[9] C.J. Madadrang, H.Y. Kim, G.H. Gao, N. Wang, J. Zhu, H. Feng, Adsorption behavior of EDTA-graphene oxide for Pb(II) removal, ACS Appl. Mater. Interfaces 4 (2012) 1186–1193.

[10] X.L. Song, J.H. Li, S.F. Xu, R.J. Ying, J. Ma, C.Y. Liao, D.Y. Liu, J.B. Yu, L.X. Chen, Determination of 16 polycyclic aromatic hydrocarbons in seawater using molecularly imprinted solid-phase extraction coupled with gas chromatography-mass spectrometry, Talanta 99 (2012) 75–82.

[11] S.F. Xu, L.X. Chen, J.H. Li, Y.F. Guan, H.Z. Lu, Novel Hg^{2+}-imprinted polymers based on thymine-Hg^{2+}-thymine interaction for highly selective preconcentration of Hg^{2+} in water samples, J. Hazard. Mater. 237 (2012) 347–354.

[12] L.X. Chen, S.F. Xu, J.H. Li, Recent advances in molecular imprinting technology: Current status, challenges and highlighted applications, Chem. Soc. Rev. 40 (2011) 2922–2942.

[13] M. Behbahani, A. Bagheri, M. Taghizadeh, M. Salarian, O. Sadeghi, L. Adlnasab, K.L. Jalali, Synthesis and characterisation of nano structure lead (II) ion-imprinted polymer as a new sorbent for selective extraction and preconcentration of ultra trace amounts of lead ions from vegetables, rice, and fish samples, Food Chem. 138 (2013) 2050–2056.

[14] J.J. Wang, X.N. Li, Ion-imprinted poly(2-acrylamido-2-methyl-1-propansulfonic acid)/modified silica composite hydrogel for selective and enhanced adsorption of Pb(II) ions, Desalin. Water Treat. 52 (2014) 274–282.

[15] X.Q. Cai, J. Li, Z. Zhong, F.F. Yang, R. Dong, L.X. Chen, Novel Pb^{2+} ion imprinted polymers based on ionic interaction via synergy of dual functional monomers for selective solid-phase extraction of Pb^{2+} in water samples, ACS Appl. Mater. Interfaces 6 (2014) 305–313.

[16] E. Yilmaz, O. Ramstrom, P. Moller, D. Sanchez, K. Mosbach, A facile method for preparing molecularly imprinted polymer spheres using spherical silica templates, J. Mater. Chem. 12 (2002) 1577–1581.

[17] H.H. Yang, S.Q. Zhang, F. Tan, Z.X. Zhuang, X.R. Wang, Surface molecularly imprinted nanowires for biorecognition, J. Am. Chem. Soc. 127 (2005) 1378–1379.

[18] F. Li, H.Q. Jiang, S.S. Zhang, An ion-imprinted silica-supported organic-inorganic hybrid sorbent prepared by a surface imprinting technique combined with a polysaccharide incorporated sol-gel process for selective separation of cadmium (II) from aqueous solution, Talanta 71 (2007) 1487–1493.

[19] M. Elena, D. Garcíá, R.B. Laío, Molecular imprinting in sol-gel materials: Recent developments and applications, Microchim. Acta 149 (2005) 19–36.

[20] W. Luo, L.H. Zhu, C. Yu, H.Q. Tang, H.X. Yu, X. Li, X. Zhang, Synthesis of surface molecularly imprinted silica micro-particles in aqueous solution and the usage for selective offline solid-phase extraction of 2,4-dinitrophenol from water matrixes, Anal. Chem. 618 (2008) 147–156.

[21] L.C.C. Silva, L.B.O. Santos, G. Abate, I.C. Cosentino, M.C.A. Fantini, J.C. Masini, J.R. Matos, Adsorption of Pb^{2+}, Cu^{2+} and Cd^{2+} in FDU-1 silica and FDU-1 silica modified with humic acid, Microporous Mesoporous Mater. 110 (2008) 250–259.

[22] A. Heidari, H. Younesi, Z. Mehraban, Removal of Ni (II), Cd(II), and Pb(II) from a ternary aqueous solution by amino functionalized mesoporous and nano mesoporous silica, Chem. Eng. J. 153 (2009) 70–79.

[23] L. Tian, G. Xie, R.X. Li, X.H. Yu, Y.Q. Hou, Removal of Cr(VI) from aqueous solution using MCM-41. Desalin. Water Treat. 36 (2011) 334–343.

[24] M. Rhazi, J. Desbrieres, A. Tolaimate, M. Rinaudo, P. Vottero, A. Alagui, M.E. Meray, Influence of the nature of the metal ions on the complexation with chitosan-application to the treatment of liquid waste, Eur. Polym. J. 38 (2002) 1523–1530.

[25] N. Viswanathan, C.S. Sundaram, S. Meenakshi, Sorption behavior of fluoride on carboxylated cross-linked chitosan beads, Colloids Surf., B 68 (2009) 48–54.

[26] C.M. Ding, W.J. Yue, Y. Su, G.Y. Li, L. Guo, L. Chen, Preparation and spectral analysis of coordination compounds of chitosan with Ce(III), Zr(IV), Pb(II) and Cd (II), Spectrosc. Spect. Anal. 27 (2007) 1185–1187.
[27] A. Burke, J. Hanrahan, D. Healy, J. Sodeau, J. Holmes, M. Morris, Large pore bifunctionalized mesoporous silica for metal ion pollution treatment, J. Hazard. Mater. 164 (2009) 229–234.
[28] A.J. Varmaa, S.V. Deshpandea, J.F. Kennedy, Metal complexation by chitosan and its derivatives a review, Carbohydr Polym. 55 (2004) 77–93.
[29] J. Li, R.B. Bai, Mechanisms of lead adsorption on chitosan/PVA hydrogel beads, Langmuir 18 (2002) 9765–9770.
[30] J.Y. Li, S.S. Shukla, K.L. Dorris, A. Shukla, J.L. Margrave, Adsorption of chromium from aqueous solutions by maple sawdust, J. Hazard. Mater. 100 (2003) 53–63.
[31] T.P. Rao, S. Daniel, J.M. Gladis, Tailored materials for preconcentration or separation of metals by ion-imprinted polymers for solid-phase extraction (IIP-SPE), Trends Anal. Chem. 23 (2004) 28–35.
[32] A.R. Iftikhar, H.N. Bhatti, M.A. Hanifa, R. Nadeem, Kinetic and thermodynamic aspects of Cu(II) and Cr (III) removal from aqueous solutions using rose waste biomass, J. Hazard. Mater. 161 (2009) 941–947.
[33] M. Özacara, I.A. Sengilb, H. Turkmenler, Equilibrium and kinetic data, and adsorption mechanism for adsorption of lead onto valonia tannin resin, Chem. Eng. J. 143 (2008) 32–42.
[34] A. Bhatnagar, A.K. Jain, A comparative adsorption study with different industrial wastes as adsorbents for the removal of cationic dyes from water, J. Colloid Interface Sci. 281 (2005) 49–55.
[35] W. Shen, S.Y. Chen, S.K. Shi, X.L. Xiang, W.L. Hu, H.P. Wang, Adsorption of Cu(II) and Pb(II) onto diethylenetriamine-bacterial cellulose, Carbohydr Polym. 75 (2009) 110–114.
[36] J.H. Huang, Y.F. Liua, Q.Z. Jina, X.G. Wanga, J. Yang, Adsorption studies of a water soluble dye, Reactive Red MF-3B, using sonication-surfactant-modified attapulgite clay, J. Hazard. Mater. 143 (2007) 541–546.
[37] C. Esen, M. Andac, N. Bereli, R. Say, E. Henden, A. Denizli, Highly selective ion-imprinted particles for solid-phase extraction of Pb^{2+} ions, Mater. Sci. Eng. J. 29 (2009) 2464–2470.
[38] X. Zhu, Y. Cui, X. Chang, X. Zou, Z. Li, Selective solid-phase extraction of lead(II) from biological and natural water samples using surface-grafted lead(II)-imprinted polymers, Microchim. Acta 16 (2009) 125–132.
[39] C. Li, J. Gao, J. Pan, Z. Zhang, Y. Yan, Synthesis, characterization, and adsorption performance of Pb(II)-imprinted polymer in nano-TiO_2 matrix, J. Environ. Sci. 21 (2009) 1722–1729.